Alignment of CN from 248 nm photolysis of ICN: A new model of the $\tilde{A}$ continuum dissociation dynamics

Maureen A. O'Halloran,[a] Hellmut Joswig,[b] and Richard N. Zare
Department of Chemistry, Stanford University, Stanford, California 94305

(Received 12 March 1987; accepted 20 March 1987)

A KrF excimer laser (248 nm) is used to dissociate a low pressure (5–10 mTorr) sample of cyanogen iodide (ICN) and the resulting CN $X\,^2\Sigma^+$ fragments are probed by laser-induced fluorescence (LIF) via various vibrational sequences of the $B\,^2\Sigma^+$–$X\,^2\Sigma^+$ transition. In addition to measuring relative vibrational and rotational populations in the CN $X\,^2\Sigma^+$ photofragment, the alignment of rotational angular momentum in this fragment is determined from the variation in LIF intensity as the direction of linear polarization of the probe laser is rotated with respect to that of the photolysis laser. A unifying model is proposed for the $\tilde{A}$ continuum photodissociation dynamics which is able to account for present and previous experimental measurements characterizing both the I and CN photofragments.

I. INTRODUCTION

The photodissociation dynamics of ICN in its near UV $\tilde{A}$ continuum has long been the object of both interest and controversy. The photodissociation of this linear triatomic has been studied for over ten years, but the complexity of this photodissociation process defies easy interpretation. Early studies demonstrated that more than one excited state is involved in the photodissociation dynamics of ICN, producing iodine atoms in the two spin–orbit states, $I^*(^2P_{1/2})$ and $I(^2P_{3/2})$, as well as highly excited and structured rotational distributions in the CN $X\,^2\Sigma^+$ fragment.[1–4] Photofragment angular distribution measurements by Ling and Wilson[1] at 266 nm, near the peak of the $\tilde{A}$ continuum, established that both components are produced through predominantly parallel transitions. The work of Pitts and Baronavski[3] showed that the production of ground state iodine is favored in both the high and low wavelength regions of the $\tilde{A}$ continuum, while the electronically excited state is favored in the central wavelength region. Hess and Leone[5] have recently remeasured $I^*(^2P_{1/2})$ quantum yields for photodissociation of ICN in the $\tilde{A}$ continuum. They find an $I^*(^2P_{1/2})$: $I(^2P_{3/2})$ ratio of 1.9 and 0.8 for photolysis at 266 and 248 nm, respectively. It is generally agreed that at least three excited electronic states of the parent ICN molecule contribute to the photodissociation in the $\tilde{A}$ continuum. It has been argued on the basis of symmetry correlation diagrams that the states which correlate with the ground state $I(^2P_{3/2})$ atom must be bent,[6] and that it is the transition from the linear ground state of the parent ICN molecule to the bent excited state(s) that produces the high degree of rotational excitation observed in the CN $X\,^2\Sigma^+$ photofragment distribution.

A number of recent studies have investigated the final state distributions of the CN photofragment in considerable detail. The vibrational and rotational distributions of the CN photofragment have been determined at a number of wavelengths throughout the $\tilde{A}$ continuum.[7–11] These studies are valuable in determining the relative contributions of different states at different wavelengths, but do not reveal whether these states are directly accessed in the initial absorption or through subsequent nonadiabatic transitions.

As a complement to the measurement of scalar quantities, such as the distributions of photofragment internal energy, the spatial distributions of vector quantities, such as velocity or angular momentum, can provide additional insight into the details of the dynamics of the photofragmentation process[12–20] The direction of linear polarization of the photolysis photon $\hat{\epsilon}_p$, introduces a laboratory fixed axis (the $\hat{Z}$ axis) about which the excited molecules, and the final distributions of photofragments, must possess cylindrical symmetry. The distribution of molecule fixed frames with respect to the laboratory fixed frame is determined by the dipole transition probability, which is proportional to $|\hat{\epsilon}_p \cdot \boldsymbol{\mu}|^2$, or to $\cos^2 \theta_\mu$, where $\boldsymbol{\mu}$ is the dipole transition moment.[14,15] The transition moment $\boldsymbol{\mu}$ depends on the symmetry of the initial and excited states relative to each other, and is fixed in the molecular frame, parallel to the internuclear axis in the limit of a purely parallel transition in a linear molecule, and perpendicular to the internuclear axis for a purely perpendicular transition. The dipole transition probability thus establishes the relationship between the molecular frame and the laboratory $\hat{Z}$ axis. Vector quantities, such as velocity or angular momentum, which are oriented with respect to the molecular frame will, therefore, have an anisotropic distribution in the laboratory frame. The tensor character of the dipole term in the Hamiltonian further determines that the spatial distributions of these vectors may be described by even multipole moments of rank $k = 0$, 2 and component $q = 0$.

The angular distribution of fragments created by electric dipole allowed photodissociation can, therefore, be described by[12,14]

$$f(\theta) = 1/4\pi\{1 + \beta P_2(\cos\theta)\},$$

where $P_2(\cos\theta)$ is the second Legendre polynomial of the angle θ between the velocity vector $\mathbf{v}$ and the $\hat{Z}$ axis, and β is a parameter determined by the photodissociation dynamics,

[a] Present address: Argonne National Laboratory, Argonne, Illinois 60439.
[b] Present address: Siemens AG, ZT MTZ 21, Otto-Hahn-Ring 6, 8000 München 83, Federal Republic of Germany.

 0021-9606/87/130303-11$02.10

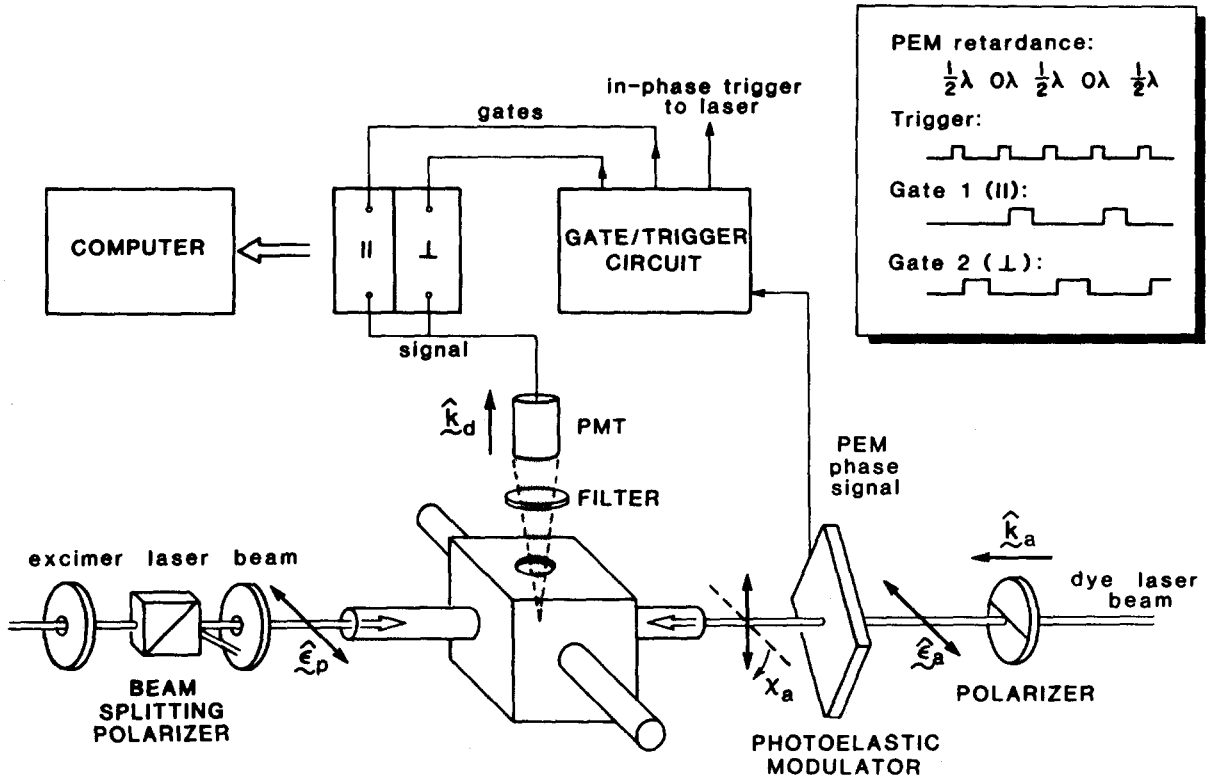

FIG. 1. Schematic diagram of apparatus used in polarization measurements. Inset shows a timing diagram for gated detection of polarization response.

with the limits $-1 \leqslant \beta \leqslant 2$. Similarly, it can be shown that the photofragment alignment, defined by[16–18]

$$\mathscr{A}_0^{(2)} = \langle (3J_z^2 - \mathbf{J}^2)/\mathbf{J}^2 \rangle$$

[proportional to the second Legendre polynomial $P_2(\cos\theta_J)$ of the angle θ_J between the angular momentum vector $\mathbf{J}$ and the $\hat{\mathbf{Z}}$ axis] has the range $4/5 \leqslant \mathscr{A}_0^{(2)} \leqslant -2/5$. For an isotropic velocity or angular momentum distribution, both β and $\mathscr{A}_0^{(2)}$ will be zero. The parameters β and $\mathscr{A}_0^{(2)}$ take their limiting values when the transition is between pure, well-defined electronic states followed by prompt dissociation with no interaction between the recoiling photofragments. Departures from these limits may, therefore, reveal information about the character of the electronic state(s), about the excited state lifetime of the parent molecule, and about the interactions between the recoiling photofragments.

The angular distributions of the CN $X\,^2\Sigma^+, v'' = 0, N''$ fragment produced at 266 nm have recently been determined by Nadler *et al.*[11] The velocity distribution of the CN photofragment, as well as the $I^*(^2P_{1/2})$:$I(^2P_{3/2})$ ratio, is determined from the shape of the Doppler profile for specific rotational levels. The state specific β parameters $\beta(N'')$ vary from 1.6 to 1.3 as a function of N'', compared to the parallel limit of 2. These results are interpreted as showing that the initial absorption is to a linear state which correlates with $I^*(^2P_{1/2})$ + CN(low N''), and is predominantly parallel. In this model, a second, bent surface which correlates with $I(^2P_{3/2})$ + CN(high N''), is populated in a subsequent nonadiabatic transition. Another study, performed by Hall *et al.*,[21] has investigated the alignment of rotational angular momentum, $\mathscr{A}_0^{(2)}(N'')$ of the CN $X\,^2\Sigma^+, v'' = 0, N''$ photofragment at a number of wavelengths. The alignment varies with rotational quantum number, but the average alignment as a function of wavelength is shown to roughly track the wavelength dependence of the $I^*(^2P_{1/2})$:$I(^2P_{3/2})$ ratio previously determined by Pitts and Baronavski.[3] These workers, therefore, offer the alternative interpretation that the different excited electronic states are directly populated in the initial absorption step.

We have undertaken a study of both the relative vibrational and rotational populations of the CN $X\,^2\Sigma^+$ photofragment produced at 248 nm, and the alignment of rotational angular momentum in that fragment. While this study has been performed at a single dissociation wavelength, our detailed examination of the final state energy distributions and alignment of the CN fragment as a function of N'' has provided us with additional evidence for the interpretation of the dynamics of the $\tilde{A}$ continuum photodissociation of ICN. We present arguments that, at least in the central portion of the $\tilde{A}$ continuum absorption, a single excited electronic state is accessed, and that the alternative final state channels are populated by subsequent curve crossings.

II. EXPERIMENTAL

Figure 1 shows a schematic diagram of the experimental setup. The photolysis source is provided by the 248 nm output of a KrF excimer laser (Lumonics TE-861). A portion of the excimer laser beam is introduced into the vacuum

chamber by reflection from a 50:50 dielectric coated beam splitter, and the remainder is used to pump a tunable dye laser (Lambda-Physik 2002E). The output of the dye laser, which is used to probe various vibrational sequences of the CN $B\,^2\Sigma^+$–$X\,^2\Sigma^+$ transition, is introduced into the vacuum chamber counterpropagating to the excimer beam, and the resulting fluorescence is collected by a photomultiplier tube (RCA 7326), which views the excitation zone through an interference filter centered on the CN $B\,^2\Sigma^+$–$X\,^2\Sigma^+$, $\Delta v = 0$ sequence. In some cases, a lens is used to improve the fluorescence collection efficiency.

The laser-induced fluorescence (LIF) signal is processed by a gated boxcar integrator (PAR 162, 164, and 165), and the voltage output is converted to a frequency, which is summed in an Ortec counter and ultimately stored in a microcomputer. An external gate/trigger circuit provides the start pulse for the excimer laser and provides gate pulses for the boxcar integrator.[22,23] The intensity of the excimer and dye laser beams can be monitored by unbiased photodiodes (EG&G FND 100-Q) carefully operated in the regime of linear response, as determined by comparison with a pyroelectric detector (Molectron J3).

The portion of the excimer beam which traverses the vacuum chamber is recollimated by a long focal length quartz lens, and the beam size is further reduced to about 0.25 cm^2 before passing through a high quality quartz window. The energy of this portion of the excimer beam is about 5 mJ. In order to measure the alignment of the CN fragment, it is necessary to control the polarization of the dye and excimer lasers. The excimer beam is 60% polarized after reflection from the dielectric beam splitter. A MgF beam splitting polarizer then divides the beam into two linearly polarized components: an undeflected beam which enters the vacuum chamber and a deflected portion which is blocked by a second aperture (Fig. 1). The polarization of the undeflected beam was determined to be greater than 96%, and the addition of a calcite crystal polarizer following the beam splitting polarizer causes no change in the polarization response of the LIF signal. The direction of polarization of the photolysis beam, denoted by $\hat{\epsilon}_p$, defines the laboratory $\hat{\mathbf{Z}}$ axis, and can be set at some angle θ_d, with respect to the direction of the detector $\hat{\mathbf{k}}_d$.

The dye laser beam can also be linearly polarized to greater than 96% either with a calcite crystal polarizer or a sheet of polarizer (Polaroid HNP'B). The direction of polarization $\hat{\epsilon}_a$ can then be rotated with a birefringent photoelastic modulator (Hinds PEMCF4), set at an angle of 45° with respect to the polarizer. The retardance of the photoelastic modulator (PEM) depends on the amplitude of its compression, and the gate/trigger circuit fires the excimer laser in synchronization with the phases of the sinusoidal compression of the PEM, so that the retardance is either zero or one half-wave, and the polarization of the dye laser is therefore either unrotated or rotated 90° on alternate shots of the excimer laser.[22,23] The same photomultiplier signal is processed by two counters, which are gated on the alternate phases of the PEM so that one counter accumulates signal corresponding to $\hat{\epsilon}_a \| \hat{\epsilon}_p$, and the other that corresponding to $\hat{\epsilon}_a \perp \hat{\epsilon}_p$.

The ICN sample (Eastman Kodak) is purified by resublimation, and its vapor is made to flow slowly through the vacuum chamber at pressures of 5–10 mTorr. Relative populations and polarization response were determined to be independent of sample pressure in this range. Dye laser intensities were chosen to avoid saturation,[24] particularly when determining the polarization response. The fluorescence collection lens was removed when polarization measurements were made.

III. RESULTS AND DISCUSSION

A. Vibrational and rotational populations

The $v'' = 0$, 1, 2, 3, and 4 vibrational levels of the CN $X\,^2\Sigma^+$ fragment have been observed utilyzing various dyes to probe the $\Delta v = +1$, -1, and -2 sequences of the CN $B\,^2\Sigma^+$–$X\,^2\Sigma^+$ transition. Portions of the spectra obtained are shown in Fig. 2. The spectra were assigned with the aid of the spectroscopic constants of Engleman,[25] and by obtaining

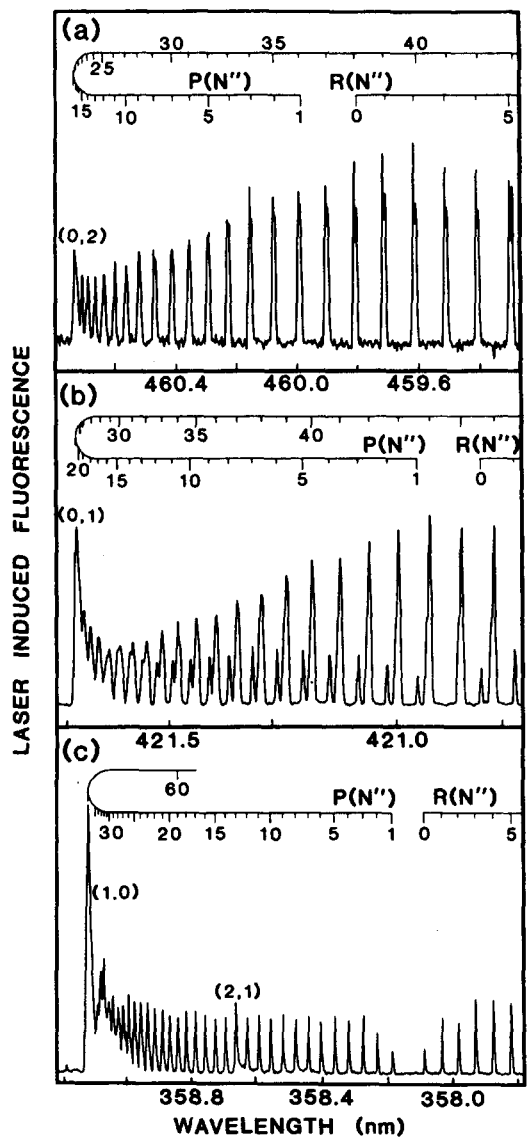

FIG. 2. Laser-induced fluorescence intensity as a function of probe laser wavelength CN $B\,^2\Sigma^+$–$X\,^2\Sigma^+$. (a) (1,0) and (2,1) bands, (b) (0,1) band. and (c) (0,2) band, following photodissociation of ICN at 248 nm. Data are uncorrected for excimer or probe laser intensities.

spectra rotationally relaxed by addition of N_2 gas where necessary. The integrated line intensities, normalized with respect to excimer and dye laser powers, were converted to relative rotational populations using the known rotational line strengths.[26] The population ratios of the various vibrational levels were then determined by comparing the intensities of either individual rovibrational levels or of the integrated bandheads, and using the knowledge of the rotational distributions and the Franck–Condon factors of Brocklehurst *et al.*[27] to calculate the relative vibrational populations.

Each rotational level N'' of the CN $X\,^2\Sigma^+$ molecule is split by spin-rotation interaction into two components F_1 and F_2 characterized by total angular momentum $J'' = N'' + 1/2$ and $J'' = N'' - 1/2$, respectively. We observe that these fine structure components are unequally populated, and that the differences in population of the two levels vary markedly with rotational quantum number N''. The population in these two components can differ by more then a factor of 2. Similar population inequalities have previously been observed by Wittig and co-workers in the photodissociation of ICN and BrCN at 266 nm.[11,28] These population inequalities prove to be an interesting feature in themselves, and a more detailed analysis is presented elsewhere.[29] The rotational populations presented here are the result of integration over both fine structure components.

The fraction of total population in each vibrational level was determined to be approximately 0.93, 0.05, 0.01, 0.004, and 0.001 for $v'' = 0$, 1, 2, 3, and 4, respectively, in good agreement with the results of Fischer *et al.*[8] The rotational distributions, obtained for $v'' = 0$, 1, and 2 are shown in Fig. 3. The technique of isolating the different vibrational levels by probing different vibrational sequences has allowed us to isolate more individual rovibrational lines than previous studies, and thus obtain a more precise determination of the rotational distributions of the higher vibrational levels. We observe that the distribution of internal energy in the CN fragment is highly nonstatistical: As the amount of energy going into vibrational increases, the amount of rotational energy increases as well. The structured rotational distribution seen in CN $X\,^2\Sigma^+$, $v'' = 0$ (Fig. 3) is characteristic of photolysis of ICN throughout the $\tilde{A}$ continuum.[4,7–11] The rotational distribution of the lowest vibrational level can be fit to three Boltzmann temperatures: $T \sim 90$, $T \sim 400$, and $T \sim 4700$ K. These agree qualitatively with the distributions obtained by Marinelli *et al.*[10] at 245 nm using a parent ICN sample cooled to about 10 K by seeded supersonic beam expansion, indicating that the rotational excitation of the CN fragment is primarily the result of the dynamics of the photofragmentation process itself, rather than the specific internal state of the parent ICN molecule.

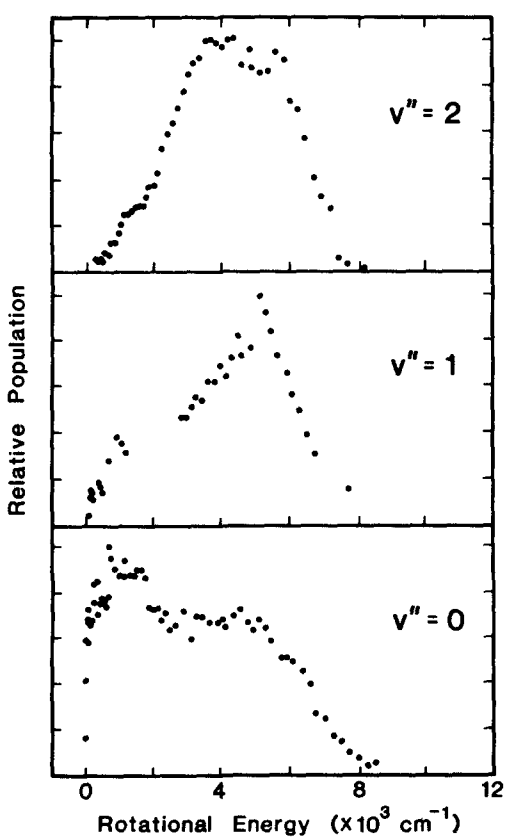

FIG. 3. Relative population as a function of rotational energy for $v'' = 0$, 1, and 2 of CN $X\,^2\Sigma^+$ produced in photodissociation of ICN at 248 nm. The population of each vibrational level is scaled so that the maximum population in any one rotational level is unity.

The rotational populations of the higher vibrational levels are also intriguing. For each higher vibrational level, the rotational "temperature" increases, and the population peaks at somewhat higher values of N'' before an increasingly sharp fall. It is interesting to note that the rotational population of each vibrational level falls off at approximately the same value of N'' (50–54), regardless of the amount of excess energy still available (~ 1 eV in the case of $v'' = 0$). This suggest that it is an angular momentum constraint, rather than energy conservation, which determines the rotational cutoff. It seems clear that the rotational state distribution of the CN fragment develops independently of the vibrational state. We will present evidence that this occurs prior to the release of the dissociation energy into vibrational and/or translational energy.

B. Alignment of the CN photofragment

We have also determined the alignment $\mathcal{A}_0^{(2)}(N'')$ of the CN $X\,^2\Sigma^+$, $v'' = 0$ photofragment as a function of rotational quantum number N''. The relationship between the spatial distribution of rotational angular momentum and the polarization dependence of laser-induced fluorescence signal has been discussed by Greene and Zare, among others.[16–20] Details of our application of their formalism are given in the Appendix. In applying this formalism, we have taken into consideration the effects of interactions of the rotational angular momentum N with the spin of the unpaired electron S and with the nuclear spin I (spin-rotation and hyperfine depolarization), which can decrease the observed polarization at low values of N''.[18,19,23] In addition, because the dye laser bandwidth is narrower than the Doppler width of the CN $B\,^2\Sigma^+$–$X\,^2\Sigma^+$ probe transition, we have also considered the effects of correlation between the direction of the photofragment velocity and the direction of its rotational angular momentum,[30] and show that although this may introduce slight discrepancies in the alignment determined in

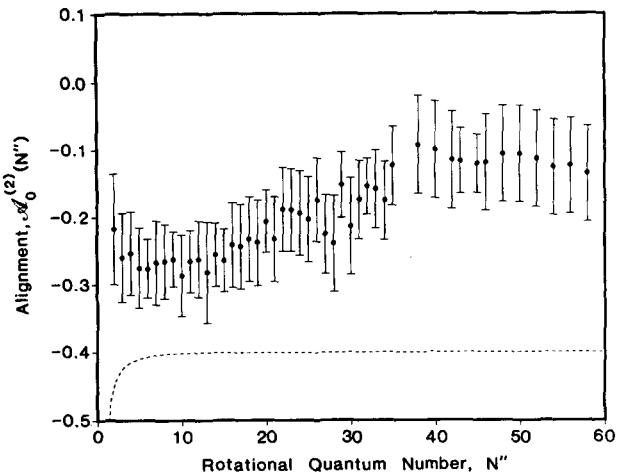

FIG. 4. Alignment $\mathscr{A}_0^{(2)}$ as a function of rotational quantum number N'', for CN $X\,^2\Sigma^+$, $v'' = 0$ from photodissociation of ICN at 248 nm. We present the average alignment determined for all observed absorption branches and experimental geometries, corrected for spin-rotation and hyperfine depolarization and for velocity-angular momentum correlations. Error bars represent statistical uncertainties in polarization response, as well as estimates of systematic uncertainties. The dashed curve represents the limiting value of the alignment for a purely parallel transition.

different experimental geometries, these are within the present experimental uncertainties.

Figure 4 shows that the alignment $\mathscr{A}_0^{(2)}(N'')$, as a function of rotational quantum number N'' for the CN $X\,^2\Sigma^+$, $v'' = 0$, N'' fragment produced in the photodissociation of ICN at 248 nm, corrected for the effects of spin-rotation and hyperfine depolarization, and for the velocity-angular momentum correlations. The error bars reflect statistical uncertainties in the polarization response translated into uncertainties in alignment, as well as estimates of systematic uncertainties. The dashed line shows the limiting value of the alignment for a purely parallel transition, calculated in the angular momentum transfer formalism.[18] For most values of N'', the dashed line approaches closely the classical limit of $-2/5$. The perpendicular limit is given by 4/5. We observe that the alignment changes with N'', from a value of about -0.28 at low N'', to about -0.12 at high N''. Our results, obtained at 248 nm with a room temperature parent ICN source, are in excellent agreement with the recent measurements of Hall *et al.*,[21] obtained at 245 nm with a supersonically cooled 10 K sample.

C. Photodissociation model

The maximum degree of alignment (or maximum photofragment ansotropy) is achieved for a purely parallel or perpendicular transition followed by prompt axial recoil of the photofragments.[13–15] For a parallel transition in a linear molecule, such as ICN, this corresponds to a transition moment $\boldsymbol{\mu}$ along the internuclear axis, a recoil velocity $\mathbf{v}$ directed along this axis, and rotational angular momentum $\mathbf{N}$ that is opposed to the orbital angular momentum, therefore, perpendicular to $\mathbf{v}$ and, hence, perpendicular to the internuclear axis. Both the alignment, $\mathscr{A}_0^{(2)}$, and the β parameter may differ from their respective limits if the transition moment is mixed, that is neither purely parallel nor purely perpendicular. In addition, any factor which causes a change in the direction of the velocity vector relative to the intial direction of the transition moment will decrease the magnitude of the β parameter. Similarly, any factor which causes a change in the direction of the angular momentum vector will decrease the magnitude of $\mathscr{A}_0^{(2)}$. A combination of different effects may reduce the values of β and $\mathscr{A}_0^{(2)}$: (1) There may be a finite predissociation lifetime of the excited molecule, which then has time to bend or rotate prior to dissociation, or (2) there may be forces between the recoiling photofragments which change the directions of the velocities and/or angular momenta of the fragments.

The fact that the alignment is the same for photodissociation of room temperature ICN as it is for dissociation of supersonically cooled ICN, indicates that the rotational and vibrational state of the ICN parent has little, if any, observable effect on the alignment of the CN fragment. The most probable rotational states of the ICN molecule at 10 and 300 K are 6 and 31, respectively, and the degree of depolarization due to a finite parent lifetime[13,15] must differ correspondingly for parent populations at the two different temperatures. Thus, the decrease in the magnitude of the alignment from its limiting value of $-2/5$ is *not* due to a finite predissociation lifetime of the excited ICN, since such as effect would be strongly dependent on the rotational state of the parent molecule.

A more direct measurement of the ICN "lifetime" has recently been performed by Scherer *et al.*[31] utilizing a femtosecond photolysis laser at 306 nm followed by femtosecond pulses at 388 nm to probe the time for appearance of the CN $B\,^2\Sigma^+$–$X\,^2\Sigma^+$ (0,0) resonant fluorescence. They determine a rise time for the appearance of the CN photofragment of 600 ± 100 fs. This is a time scale which would cause a greater degree of decrease in the β parameter or alignment than is experimentally observed, if the excited ICN were allowed to rotate for the entire time. It must be realized, however, that the "clock" that is used to measure this lifetime is sensitive to the separation of the I and CN fragments and the change in the CN bond length, and not to the bending in the ICN bond and the development of the CN rotation. We conclude that the bending of the ICN, and, therefore, the dynamics that produce the rotational excitation of the CN fragment, take place on a much shorter time scale than the dynamics involving the I–CN recoil and the development of the CN vibrational state. This is in keeping with the observation that the rotational cutoff in the CN $X\,^2\Sigma^+$ fragment is relatively independent of vibrational energy, occurring well before the energetic cutoff in the lower vibrational levels.

Hall, Sivakumar, and Houston[21] have also determined the alignment of the CN photofragment resulting from photodissociation of ICN at several different wavelengths in the $\tilde{A}$ continuum. They interpreted their data to show that the average alignment as a function of wavelength roughly tracks the $I^*(^2P_{1/2})$:$I(^2P_{3/2})$ ratio. However, they did not measure the alignment at the same values of N'' for all wavelengths. Our more detailed determination of the alignment at a single wavelength as a function of N'' shows that because of the variation in alignment with N'', it is not valid to compare alignments for different values of N'' obtained at different wavelengths. If we look at their table of alignment data

(Table I, Ref. 21), we see that the magnitudes of the alignments at nearby values of N'' are constant in the range 245–266 nm, and in contradiction to their conclusions, do not track the $I^*(^2P_{1/2})$:$I(^2P_{3/2})$ ratio, which varies by over a factor of 2 in this wavelength range.[5]

The observed change in alignment with N'', presented in Fig. 4, may result from the superposition of two rotational distributions—one component peaked at low N'', which has an alignment of -0.28, and another, peaked at high N'', with an alignment of -0.12. In the recent experimental determination of the angular distributions of the CN photofragments produced in photodisociation of ICN at 266 nm, Nadler *et al.*[11] found that the β parameter varied with N'' in a similar fashion. Their angular distributions were determined from the shape of the CN Doppler profile. They were able to extract the β parameters, and also to separate out, from the differences in the width of the Doppler profiles, the CN fragments produced in correlation with $I^*(^2P_{1/2})$ from those produced in correlation with $I(^2P_{3/2})$. They determined a β parameter of 1.6 for the low N'' component, which is correlated with $I^*(^2P_{1/2})$, and a β parameter of 1.3 for the high N'' component, which is correlated with $I(^2P_{3/2})$. No correction was made for velocity-angular momentum correlations, but for the geometry used, these are expected to be small. This suggest that our variation in alignment is produced by a similar final state distribution. This would indicate a production of $I^*(^2P_{1/2})$ at this wavelength greatly in excess of the 14% reported by Pitts and Baranavski,[3] and in fact a ratio of $44 \pm 4\%$ has recently been determined by Hess and Leone.[5]

Based on an unpublished magnetic circular dichroism (MCD) study of Gedanken, Nadler *et al.*[11] argued that only one ICN electronic state is directly accessed throughout the $\tilde{A}$ continuum. They interpret their β parameter measurements at 266 nm as showing that the initial absorption is to a linear state correlating with $I^*(^2P_{1/2}) + CN(\text{low } N'')$, having predominantly parallel character, which subsequently crosses a bent state correlating with $I(^2P_{3/2}) + CN(\text{high } N'')$. The slight decrease in the β parameter of the rotationally excited component relative to the colder component is then explained by the change in direction of the velocity vector resulting from bending of the ICN molecule.

The problem with such a picture is that bending of the ICN molecule, which changes the direction of the velocity vector, may change the magnitude of the rotational angular momentum **N**, but will *not* change its direction. The rotation of the CN fragment remains opposed to the orbital angular momentum, and thus perpendicular to the ICN plane, regardless of the amount of bending of the molecule. Thus, in this simple picture, we would expect a decrease in the β parameter, but no decrease in the magnitude of the alignment following a curve crossing from a linear to a bent surface. This is in contradiction to the present work in which we find a decrease in the alignment of the rotationally excited component that is at least as large as the change in the β parameters for the two components observed at 266 nm.

We propose an alternative model which would account for the variation of both β and $\mathscr{A}_0^{(2)}$ with N''. It is clear that at least two excited states are involved in the $\tilde{A}$ continuum dissociation of ICN: a linear state correlating with $I^*(^2P_{1/2})$ and CN $X\,^2\Sigma^+$ with low values of the rotational quantum number N'' and a bent state correlating with $I(^2P_{3/2})$ and rotationally excited CN $X\,^2\Sigma^+$. Franck–Condon factors will favor transitions from the linear ground state of ICN to the linear excited state, so that the initial transition is to the surface correlating with $I^*(^2P_{1/2})$. It is the torque involved in the nonadiabatic transition to the bent potential energy surface and subsequent trajectory on that surface which causes rotational excitation of the CN $X\,^2\Sigma^+$ fragment correlating with $I(^2P_{3/2})$. This is the same conclusion that was reached by Nadler *et al.*,[11] and is supported by Gedanken's MCD data. We suppose that the dynamics of the curve crossing between the linear and the bent surfaces take place in the region of small I–CN separation, i.e., in the Franck–Condon region directly above the well of the bound parent molecule, so that there are strong, nonplanar interactions between the developing CN rotation **N** and the nuclear spin or electronic orbital angular momentum of the iodine atom. These nonplanar forces change the directions of *both* the velocity and angular momentum vectors, thus, causing a decrease in the magnitude of both the β parameter and the alignment $\mathscr{A}_0^{(2)}$. This model is supported by our earlier conclusion that the CN rotation develops on a very short time scale, prior to the release of energy into vibration or translation.

There is, in fact, definitive evidence for the existence of nonplanar, spin-dependent forces in the photodissociation of ICN.[29] In order for the observed differences in the population of the spin-rotation components of the CN fragment to exist, that is in order for the rotation **N** of the CN fragment to have a preferred orientation with respect to the spin **S** of the unpaired electron, there must be nonplanar forces that will align the developing rotation **N** relative to **S**. We observe such population differences in the two spin-rotation components of the CN photofragment, which vary with photolysis wavelength and with rotational quantum number, and may differ by more than a factor of 2.[5] The variation with N'' is attributed to quantum interference between wave packets traveling on different potential energy surfaces correlating with the same observable final states. Our model calculations, which determine the WKB phases accumulated on the alternative dissociation paths, both leading to ground state $I(^2P_{3/2})$ and CN, $v'' = 2$, N'', show that the wavelength dependence of the population inequalities are best matched by surfaces which cross near the Franck–Condon region.

Further support for strong coupling between the excited ICN surfaces at short distances is provided by the recent work of Goldfield *et al.*[32] Their calculation, which was the first to introduce nonadiabatic interactions between the various ICN surfaces into a classical trajectory calculation, showed that strong coupling between the surfaces in the Franck–Condon region is also necessary in order to explain the wavelength dependence of the $I^*(^2P_{1/2})$:$I(^2P_{3/2})$ ratio and of the rotational distributions. In summary, the observed rotational distributions as well as the variations in both β and $\mathscr{A}_0^{(2)}$ with N'' can be qualitatively explained by a single model which invokes nonadiabatic crossings in the Franck–Condon region of the dissociative transition.

ACKNOWLEDGMENT

This work was supported by the National Science Foundation under Grant No. NSF PHY 85-06668.

APPENDIX: DETERMINATION OF ALIGNMENT FROM POLARIZATION MEASUREMENTS

The physical basis for the determination of the spatial distribution of rotational angular momentum in a molecule is the dependence of the probability of absorption or emission of light upon the orientation of the molecular rotation relative to the directions of propagation and polarization of the absorbed or emitted photons. This has been discussed by Case, McClelland, and Herschbach,[17] by Bain and McCaffery,[20] by Fano and Macek,[16] and by Greene and Zare.[18,19] We follow the latter two sources, in which the spatial distribution of angular momentum, i.e., the J_Z distribution, is expanded in multipole moments $\mathscr{A}_q^{(k)}(J)$ in order to exploit the symmetry of the experimental configuration. The intensity of laser-induced fluorescence signal for a probe transition $J_i \rightarrow J_e$, followed by detection of fluorescence $J_e \rightarrow J_f$, is then given by[19]

$$I = CS \sum_{k_d,k_a,k,q} \mathscr{A}_q^{(k)}(J_i)\epsilon(k_d,k_a,k,q;\Omega)\omega(k_d,k_a,k;J_i,J_e,J_f). \tag{A1}$$

Here C is a proportionality constant, the factor S is the product of the electronic line strength and Franck–Condon factors, the factors $\epsilon(k_d,k_a,k,q;\Omega)$ depend on the physical geometry of the experiment ($\Omega \equiv \phi_a,\theta_a,\chi_a,\phi_d,\theta_d,\chi_d$, as defined in Ref. 19), the factors $\omega(k_d,k_a,k;J_i,J_e,J_f)$ depend on the particular probe absorption and emission steps $J_i \rightarrow J_e \rightarrow J_f$, and $\mathscr{A}_q^{(k)}(J_i)$ are the multipole moments of the intial angular momentum distribution. At this point, J simply denotes the angular momentum quantum number of the molecule, and no distinction is made between the rotational angular momentum quantum number N and the total angular momentum quantum number J. The sum is over k_d and $k_a = 0,2$ with k_d and k_a being required to sum to k in the sense of addition of angular momenta, so that regardless of the angular momentum distribution, the LIF probe is sensitive only to moments $\mathscr{A}_q^{(k)}$ up to rank $k = 4$.

A cylindrically symmetric angular momentum distribution will possess only moments with $k =$ even and $q = 0$. Moreover, if the distribution is created by a dipole process, then only net moments up to $k = 2$ will be present. Thus, in the case of an angular momentum distribution created by (electric-dipole-allowed) photodissociation by linearly polarized light, the LIF intensity will depend in principle only on the moments $\mathscr{A}_0^{(0)}$ and $\mathscr{A}_0^{(2)}$, i.e., on the population and the quadrupole alignment. The intensities observed at two different experimental geometries can, therefore, be used to extract these two moments.

This procedure assumes that the method of detection does not itself break the cylindrical symmetry of the angular momentum distribution. This can be true if the probability of detection depends only on the polar angle measured from the laboratory Z axis. However, if the probe laser linewidth is narrower than the Doppler width of the photofragment transition, then this cylindrical symmetry is partially broken, since the probe laser will detect only those fragments with a limited set of velocity projections on the probe direction (Fig. 5). In what follows, we first treat the case of full cylindrical symmetry, then consider the bias introduced by the finite probe laser bandwidth.

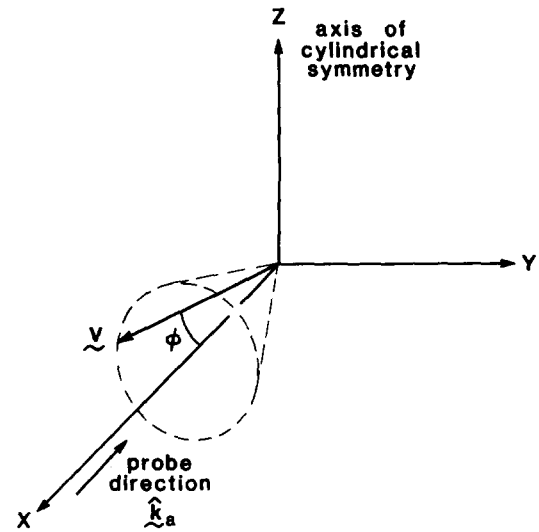

FIG. 5. Diagram of the excitation-detection geometry, illustrating that the probe laser breaks the cylindrical symmetry of the photofragment distribution by sampling only a limited range of photofragment velocity components.

1. Excitation-detection geometry and unresolved emission

To achieve these changes in geometry necessary to extract $\mathscr{A}_0^{(2)}$ relative to $\mathscr{A}_0^{(0)}$, we rotate the direction of polarization of the probe laser $\hat{\epsilon}_a$, with respect to that of the photolysis laser $\hat{\epsilon}_p \equiv \hat{Z}$, and measure the LIF intensity at the two angles $\chi_a = 0 (\hat{\epsilon}_a \| \hat{\epsilon}_p)$ and $\chi_a = \pi/2$ ($\hat{\epsilon}_a \perp \hat{\epsilon}_p$), defining a polarization response P as

$$P = \frac{I_\parallel - I_\perp}{I_\parallel + I_\perp}, \tag{A2}$$

where $I_\parallel$ and $I_\perp$ are the LIF intensities measured with the dye laser polarization $\hat{\epsilon}_a$ parallel or perpendicular with respect to the direction of polarization of the photolysis laser $\hat{\epsilon}_p$, respectively. Our detector is insensitive to the polarization of the fluorescence, and so we must sum the intensities over the detector polarization angles $\chi_d = 0$ and $\chi_d = \pi/2$. In addition, the fluorescence is unresolved, so we sum over the P, Q, and R branches in emission. For a Σ–Σ transition, the satellite Q branches only have intensity for the lowest rotational levels. We define

$$\bar{\epsilon}(k_d,k_a,k,q;\Omega) \equiv \epsilon[k_d,k_a,k,q;\Omega(\chi_d = 0)] + \epsilon[k_d,k_a,k,q;\Omega(\chi_d = \pi/2)] \tag{A3}$$

and

$$\bar{\omega}(k_d,k_a,k;J_i,J_e) = \sum_{J_f} S(J_e,J_f)\omega(k_d,k_a,k;J_i,J_e,J_f), \tag{A4}$$

where $S(J_e, J_f)$ are the rotational line strengths for the different emission branches.[26] Then the LIF intensity is given by

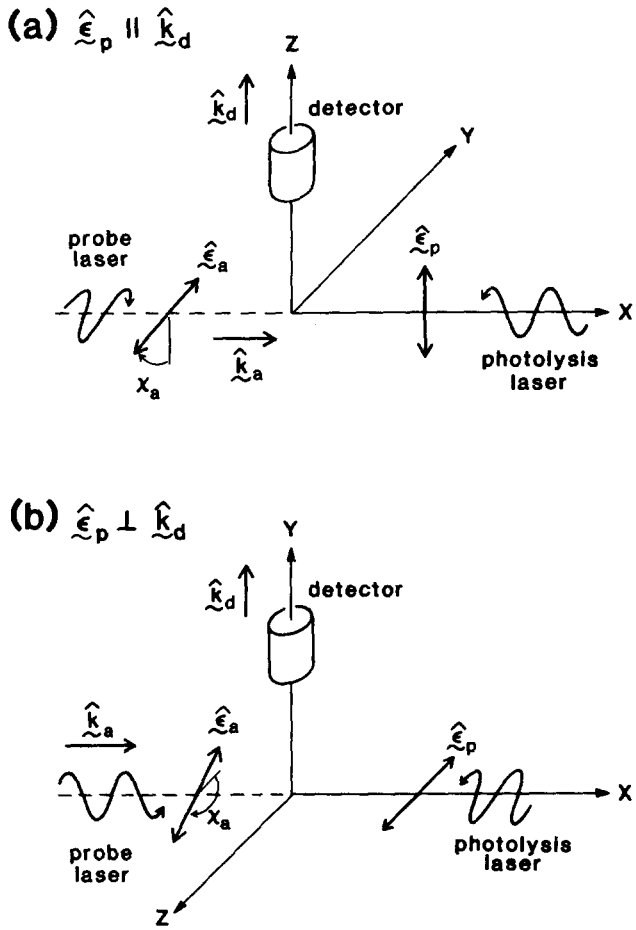

FIG. 6. Two excitation-detection geometries used to determine the photofragment alignment.

$$I = CS \sum_{k_d,k_a,k,q} \mathscr{A}_q^{(k)}(J_i)\bar{\epsilon}(k_d,k_a,k,q;\Omega)\bar{\omega}(k_d,k_a,k;J_i,J_e). \tag{A5}$$

Polarizations were measured for two different experimental geometries: One with the polarization of the photolysis laser parallel to the direction of the detector $\hat{\epsilon}_p \| \hat{k}_d$ [Fig. 6(a)] and the other with the polarization perpendicular to the detector $\hat{\epsilon}_p \perp \hat{k}_d$ [Fig. 6(b)]. The geometric factors $\bar{\epsilon}(k_d,k_a,k,q;\Omega)$ and the factors $\bar{\omega}(k_d,k_a,k;J_i,J_e)$ are explicitly calculated as described in Ref. 19, and the polarizations can then be inverted to yield the alignment $\mathscr{A}_0^{(2)}(J_i)$.

2. Depolarization by unresolved fine and hyperfine structure

When a molecule possesses either spin-rotation or hyperfine structure, then the preceding analysis is insufficient to describe the dependence of the LIF intensity on rotational alignment. If the nuclear and electronic spins do not interact with the dipole process, then the initial excitation will align only the rotational angular momentum **N** and this vector will subsequently precess about the total angular momentum. If we can assume Hund's case $b_{\beta J}$ coupling,[33] which is appropriate for $^{12}C^{14}N\,X\,^2\Sigma^+$, where the spin-rotation interaction is large compared to the hyperfine interaction, then the nuclear rotation **N** couples to the spin of an unpaired electron, $S = 1/2$ to form a total $\mathbf{J} = \mathbf{N} + \mathbf{S}$, which in turn couples to the nuclear spin $I = 1$, to form the "good" quantum number of the state F which has total angular momentum $\mathbf{F} = \mathbf{I} + \mathbf{J}$. Thus although **N** will be aligned by the absorption of the photon, this alignment will change as a function of time as **N** precesses in space.[34]

If the time between the initial excitation and the absorption of the probe photon is large compared to the period of fine structure precession, then the observed alignment is reduced according to[18,23]

$$\mathscr{A}_0^{(2)}(N_i,\text{obs}) = \mathscr{A}_0^{(2)}(N_i)g^{(2)}(N_i), \tag{A6}$$

where

$$g^{(k)}(N) = \sum_{J,F} \frac{(2F+1)^2(2J+1)^2}{(2S+1)(2I+1)} \begin{Bmatrix} J & J & k \\ N & N & S \end{Bmatrix}^2 \begin{Bmatrix} J & J & k \\ N & N & I \end{Bmatrix}^2. \tag{A7}$$

The presence of fine structure in the excited state also affects the alignment of **N** in the time between the absorption of the probe photon and the emission of the detected photon. Accordingly, each factor $\omega(k_d,k_a,k;N_i,N_e,N_f)$ must also be multiplied by a factor $g^{(k_d)}(N_e)$.[19]

Only when N is comparable to I (or S) need fine structure depolarization be taken into account. For the lowest values of N, this effect is significant, due to the presence of depolarization in both the ground and excited states of the molecule. The depolarization correction is also dependent on experimental geometry, since the alignment of the excited state will be geometry dependent, and the factors $g^{(k_d)}(N_e)\omega(k_d,k_a,k;N_i,N_e,N_f)$ appear within the coupled set of equations that must be solved to determine $\mathscr{A}_q^{(k)}(J_i)$ [Eq. (A1)]. In our case, the hyperfine and spin-rotation affects the polarization response up to values of $N'' \approx 10$.

Figure 7 presents the polarization response P, measured in the P and R branches of the CN $B\,^2\Sigma^+$–$X\,^2\Sigma^+$ (1,0) transition, for the two experimental geometries: (1) $\hat{\epsilon}_P \| \hat{k}_d$ and (2) $\hat{\epsilon}_p \perp \hat{k}_d$. The depolarization correction appropriate to

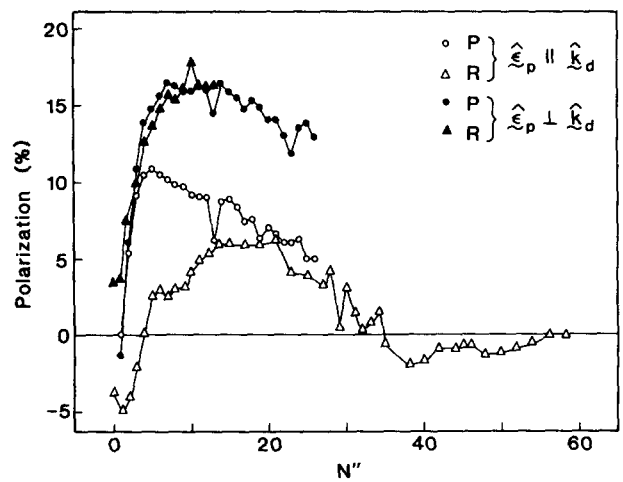

FIG. 7. Polarization response observed as the probe laser is rotated with respect to the photolysis laser for CN $X\,^2\Sigma^+$, $v'' = 0$ from photodissociation of ICN at 248 nm, as a function of rotational quantum number N''. Polarization response, defined in the text, is labeled P or R according to whether it is probed in the P or R branches of the CN $B\,^2\Sigma^+$–$X\,^2\Sigma^+$ (1,0) band, and $\hat{\epsilon}_p \| \hat{k}_d$ or $\hat{\epsilon}_p \perp \hat{k}_d$ to indicate the excitation-detection geometry.

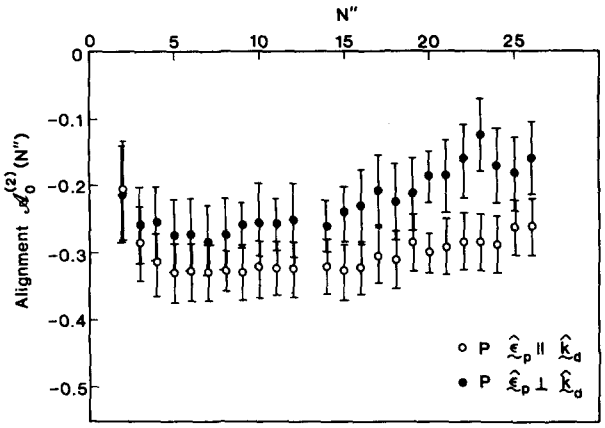

FIG. 8. Alignment $\mathscr{A}_0^{(2)}$ as a function of rotational quantum number N'', for CN $X\,^2\Sigma^+$, $v'' = 0$ from photodissociation of ICN at 248 nm. Detection is in the P branch of the CN $B\,^2\Sigma^+$–$X\,^2\Sigma^+$ (1,0) band for the geometries $\hat{\epsilon}_p \| \hat{k}_d$ and $\hat{\epsilon}_p \perp \hat{k}_d$. Error bars represent measured uncertainties in polarization response converted into uncertainties in alignment.

case b_{BJ} has been applied to the data, and the alignment $\mathscr{A}_0^{(2)}(N'')$ determined for the CN $X\,^2\Sigma^+$, $v' = 0$ photofragment produced in photodissociation of ICN at 248 nm are shown in Fig. 8, as a function of rotational quantum number for $N'' = 2$ through 25 for the two different excitation-detection geometries. The data shown are for excitation of the P branch, the data for the R branch are similar. Although the data sets for the two detection geometries nearly overlap, we see a systematic discrepancy. These discrepancies are outside what would be expected from small misalignments of the experimental geometry; it would require a change in one polarizer angle of about 20° to reconcile the two sets of data.

3. Correction for velocity-angular momentum correlation

Recall that the *net* angular momentum distribution created by the dipole photodissociation process can only have moments $\mathscr{A}_0^{(0)}$ and $\mathscr{A}_0^{(2)}$. However, the probe laser, because it is narrower than the Doppler width of the transition, does not observe the total distribution of photofragments, but rather detects only those molecules having particular velocity projections $v\cos\phi$ on the probe direction $\hat{k}_a$ (Fig. 5). In the photodissociation of ICN, we expect correlations between velocity and angular momentum directions; since the rotational angular momentum is a product of the dynamics of the photodissociation process, it will be nearly opposed to the orbital angular momentum between the fragments. Thus, we expect N to be essentially perpendicular to the velocity v. When the probe laser breaks the cylindrical symmetry of the angular momentum distribution by selecting a particular subset of velocity projections, it observes an angular momentum distribution no longer possessing cylindrical symmetry, but rather reflection symmetry through the plane defined by the direction of polarization of the photolysis laser $\hat{\epsilon}_p$ and the direction of propagation of the probe laser $\hat{k}_a$.

The moments which can contribute to the LIF intensity are then those with even k and even q. These moments depend on the angular distribution of photofragments, the angular momentum distribution, and the correlations between these two vectors. The form of $\mathscr{A}_q^{(k)}(x_D)$, as a function of the relative Doppler shift $x_D \equiv \Delta\nu/\nu_0$, has been derived by Dixon.[30] Figure 9 shows the moments $\mathscr{A}_q^{(k)}(x_D)$ for a purely parallel velocity distribution in the axial recoil limit (that is, $\cos^2\theta$ distribution of velocity vectors about the laboratory $\hat{Z}$ axis), a probe direction $\hat{k}_a \perp \hat{\epsilon}_p$, and a velocity-angular momentum correlation of v⊥N. To evaluate the dependence of the observed angular momentum distribution on the probe laser bandwidth, we have modeled the frequency profile of the probe laser by a square of relative width Δx centered on the Doppler profile, and calculated the integrated moments

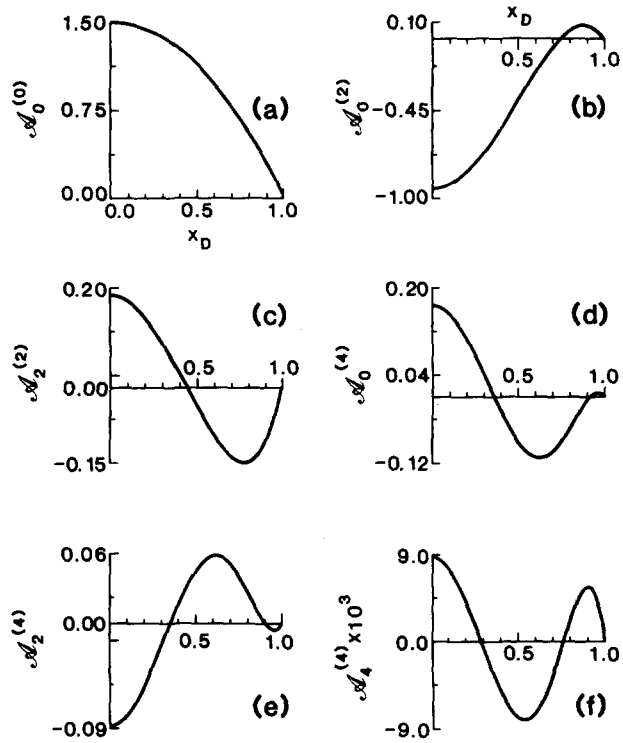

FIG. 9. Moments of the angular momentum distribution $\mathscr{A}_q^{(k)}$ as a function of relative Doppler shift x_D calculated for a parallel transition, with detection geometry $\hat{k}_a \perp \hat{\epsilon}_p$, and velocity-angular momentum correlation v⊥N.

$$\overline{\mathscr{A}_q^{(k)}}(\Delta x) = \int_{-\Delta x/2}^{\Delta x/2} \mathscr{A}_q^{(k)}(x_D)\,dx_D. \qquad \text{(A8)}$$

The results are plotted in Fig. 10, where the higher moments have been normalized to $\overline{\mathscr{A}_0^{(0)}}(\Delta x)$. Our experimental situation corresponds to a laser width of about 60% of the Doppler width of the probe transition. We find that these moments are approaching their limiting values, but that $\overline{\mathscr{A}_0^{(2)}}$ is slightly greater than the limiting value of -0.4, and that there may be a small contributions from the higher moments $\overline{\mathscr{A}_2^{(2)}}$, $\overline{\mathscr{A}_0^{(4)}}$, $\overline{\mathscr{A}_2^{(4)}}$, and $\overline{\mathscr{A}_4^{(4)}}$. For the two different experimental geometries, the moments $\mathscr{A}_q^{(k)}$ are differently weighted by the geometrical factors $\bar{\epsilon}(k_d,k_a,k,q;\Omega)$. Figure 11 shows the variation in polarization response $P(x_D)$ across the laser profile, calculated in the high J limit for the velocity-angular momentum distributions described above. The average polarization response P, obtained by integrating

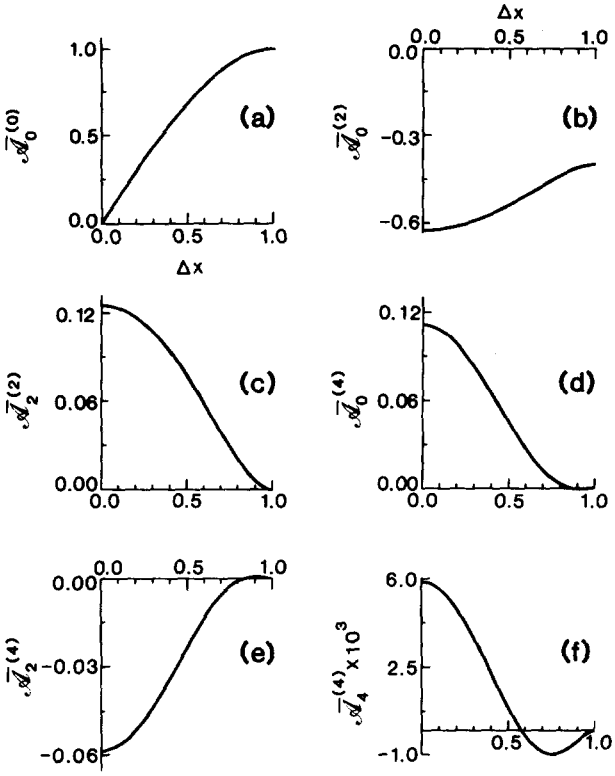

FIG. 10. Integrated moments of the angular momentum distribution $\bar{\mathscr{A}}_q^{(k)}$ as a function of probe laser bandwidth, Δx assuming a square frequency profile centered on the probe transition.

$P(x_p)$ across the entire Doppler profile, is 10.3% for the $\hat{\epsilon}_p \| \hat{\mathbf{k}}_d$ geometry and 21.2% for the $\hat{\epsilon}_p \perp \hat{\mathbf{k}}_d$ geometry. When the polarization response is converted into alignment, the limiting value of -0.40 is determined for either geometry. If the polarization is integrated over only 60% of the Doppler profile, however, the observed values of the polarization will be 12.8% and 21.7%, for the $\hat{\epsilon}_p \| \hat{\mathbf{k}}_d$ and $\hat{\epsilon}_p \perp \hat{\mathbf{k}}_d$ geometries, respectively. If the higher moments ($k > 2$ or $q > 0$) are neglected, then the alignments determined from these polarizations are -0.45 and -0.41, respectively, for the two geometries. The difference is comparable to the observed discrepancies between the alignments determined for the two experimental geometries. The corrections for velocity-angular correlation (0.05 for $\hat{\epsilon}_p \| \hat{\mathbf{k}}_d$ and 0.01 for $\hat{\epsilon}_p \perp \hat{\mathbf{k}}_d$) are within the experimental uncertainty. We apply these corrections to our data merely to remove the systematic discrepancies between the alignments determined in different experimental geometries. Figure 4 shows the weighted average of the experimentally determined alignment $\mathscr{A}_0^{(2)}(N'')$ corrected for spin-rotation and hyperfine depolarization, and for velocity-angular momentum correlation.

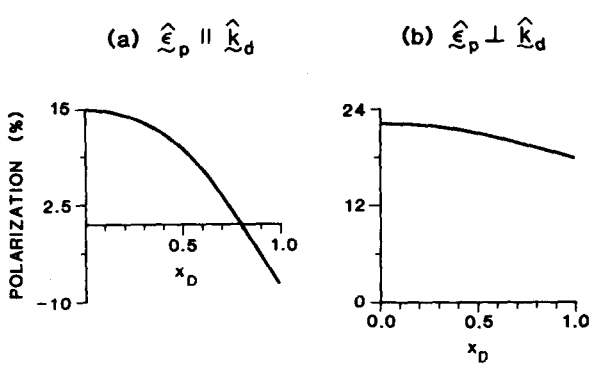

FIG. 11. Calculated polarization response P as a function of relative Doppler shift x_D.

We have not attempted to determine the various moments of the angular momentum distribution and the velocity-angular momentum correlation. It is well to keep the possible contributions from the higher moments in mind, however, when comparing data measured in different experimental configurations. If the velocity-angular momentum correlations are of interest, they may be more directly observed by probing the photofragment with a narrower bandwidth laser that does not average over so much of the Doppler profile. Several recent experiments have taken advantage of this to extract information about velocity-angular momentum correlations from the shapes of Doppler profiles.[35–37]

[1]J. H. Ling and K. R. Wilson, J. Chem. Phys. **63**, 101 (1975).
[2]A. P. Baronavski and J. R. McDonald, Chem. Phys. Lett. **45**, 172 (1977).
[3]W. M. Pitts and A. P. Baronavski, Chem. Phys. Lett. **71**, 395 (1980).
[4]A. P. Baronavski, Chem. Phys. **66**, 217 (1982).
[5]W. P. Hess and S. R. Leone, J. Chem. Phys. **86**, 3773 (1987).
[6]M. D. Morse, K. F. Freed, and Y. B. Band, J. Chem. Phys. **70**, 3620 (1979).
[7]W. H. Fischer, T. Carrington, S. V. Filseth, C. M. Sadowski, and C. H. Dugan, Chem. Phys. **82**, 443 (1983).
[8]W. H. Fischer, R. Eng, T. Carrington, C. H. Dugan, S. V. Filseth, and C. M. Sadowski, Chem. Phys. **89**, 457 (1984).
[9]I. Nadler, H. Reisler, and C. Wittig, Chem. Phys. Lett. **103**, 451 (1984).
[10]W. J. Marinelli, N. Sivakumar, and P. L. Houston, J. Phys. Chem. **88**, 6685 (1984).
[11]I. Nadler, D. Mahgerefteh, H. Reisler, and C. Wittig, J. Chem. Phys. **82**, 3885 (1985).
[12]J. Cooper and R. N. Zare, Lectures Theor. Phys. **11**, 317 (1969).
[13]C. Jonah, J. Chem. Phys. **55**, 1915 (1971).
[14]R. N. Zare, Mol. Photochem. **4**, 1 (1972).
[15]S. Yang and R. Bersohn, J. Chem. Phys. **61**, 4400 (1974).
[16]U. Fano and J. H. Macek, Rev. Mod. Phys. **45**, 265 (1973).
[17]D. A. Case, G. M. McClelland, and D. R. Herschbach, Mol. Phys. **35**, 541 (1978).
[18]C. H. Greene and R. N. Zare, Annu. Rev. Phys. Chem. **33**, 119 (1982).
[19]C. H. Greene and R. N. Zare, J. Chem. Phys. **78**, 6741 (1983).
[20]A. J. Bain and A. J. McCaffery, J. Chem. Phys. **80**, 5883 (1984).
[21]G. E. Hall, N. Sivakumar, and P. L. Houston, J. Chem. Phys. **84**, 2120 (1986).
[22]J. A. Guest, M. A. O'Halloran, and R. N. Zare, J. Chem. Phys. **81**, 2689 (1984).
[23]J. A. Guest, M. A. O'Halloran, and R. N. Zare, Chem. Phys. Lett. **103**, 261 (1984).
[24]R. I. Altkorn and R. N. Zare, Annu. Rev. Phys. Chem. **35**, 265 (1984).
[25]R. Engleman, Jr., J. Mol. Spectrosc. **49**, 106 (1974).
[26]G. Herzberg, *Molecular Spectra and Molecular Structure I. Spectra of Diatomic Molecules* (Van Nostrand Reinhold, New York, 1950), p. 208.
[27]B. Brocklehurst, G. R. Hebert, S. H. Innanen, R. M. Seel, and R. W. Nicholls, *Identification Atlas of Molecular Spectra 9* (York University Centre for Research in Experimental Space Science, Toronto, 1972).
[28]F. Shokoohi, S. Hay, and C. Wittig, Chem. Phys. Lett. **110**, 1 (1984).
[29]H. Joswig, M. A. O'Halloran, R. N. Zare, and M. S. Child, Faraday Discuss. Chem. Soc. (in press).
[30]R. N. Dixon, J. Chem. Phys. **85**, 1866 (1986).

[31]N. F. Scherer, J. L. Knee, D. D. Smith, and A. H. Zewail, J. Phys. Chem. **89**, 5141 (1985).
[32]E. M. Goldfield, P. L. Houston, and G. S. Ezra, J. Chem Phys. **84**, 3120 (1986).
[33]C. H. Townes and A. L. Schawlow, *Microwave Spectroscopy* (Dover, New York, 1975).
[34]R. I. Altkorn, R. N. Zare, and C. H. Greene, Mol. Phys. **55**, 1 (1985).
[35]G. E. Hall, N. Sivakumar, and P. L. Houston, Phys. Rev. Lett. **56**, 1671 (1986).
[36]G. E. Hall, N. Sivakumar, R. Ogorzalek, G. Chawla, H. Haerri, P. L. Houston, I. Burak, and J. W. Hepburn, Faraday Discuss. Chem. Soc. (in press).
[37]K-H. Gericke, S. Klee, F. J. Comes, and R. N. Dixon, J. Chem. Phys. **85**, 4463 (1986).